ISSN 1063-7834, Physics of the Solid State, 2019, Vol. 61, No. 3, pp. 379–382. © Pleiades Publishing, Ltd., 2019.
Russian Text © G.N. Churilov, A.I. Dudnik, N.A. Drokin, N.G. Vnukova, V.S. Bondarev, V.I. Elesina, 2019, published in Fizika Tverdogo Tela, 2019, Vol. 61, No. 3, pp. 510–513.



# Electrical Parameters of Materials Based on Modified Endohedral Metallofullerenes

**G. N. Churilov[a, b, *], A. I. Dudnik[a, b], N. A. Drokin[a], N. G. Vnukova[a, b], V. S. Bondarev[a, b], and V. I. Elesina[a, b]**

[a] *Kirensky Institute of Physics, Krasnoyarsk Scientific Center, Siberian Branch, Russian Academy of Sciences, Krasnoyarsk, 660036 Russia*
[b] *Siberian Federal University, Krasnoyarsk, 660041 Russia*
**e-mail: churilov@iph.krasn.ru*

Received October 23, 2018

**Abstract**—The film based on hydroxylated endohedral metallofullerenes with Y has been investigated. It is shown that the obtained film is an ion conductor and can behave as a ferroelectric.

**DOI:** 10.1134/S1063783419030089

Endohedral metallofullerene (EMF) molecules exhibit some features of the atomic structure. As in conventional fullerenes, carbon atoms are located on a quasi-spherical surface and have a common π system of electrons. At the same time, there is a guest atom located inside the frame and positioned at the surface. Two or three valence electrons of this atom (or molecule) usually also belong to the common π system.

The EMF-based substances are interesting for both fundamental research and application [1–4]. There has been a vast literature discussing the possibility of using modified fullerenes as, e.g., solid electrolytes, contrast agents for magnetic resonance imaging, or antiviral and anticancer drug precursors [5–7].

In contrast to fullerene molecules with an empty frame, the electrical properties of the modified EMFs have been understudied [8, 9]. This is caused by the complexity of their fabrication and extraction in amounts sufficient for experimental investigations. We developed a technique for fabricating a carbon condensate (CC) in the high-frequency arc discharge with a high content of EMFs with Y [10, 11]. Using this technique and modern EMF extraction methods, we obtained a composite of endohedral metal fullerenes $Y@C_{82}$, $Y_2@C_{82}$ with minor $Y_2C_2@C_{82}$ admixtures, and higher fullerenes in amounts sufficient for forming a film. The EMF enrichment was performed by a method based on the use of the Lewis acid $TiCl_4$ [12]. The obtained fullerene mixture sample was certified on a Bruker Biflex MALDI-TOF TM III mass spectrometer (Fig. 1).

The obtained EMFs were modified by boiling in the concentrated $HNO_3$ acid [13]. As a result, an aqueous solution of hydroxylated EMFs with Y was obtained. The solution droplets were put on a measuring sensor in the form of a plane interdigitated metallic structure on a polycor substrate. During putting droplets, the solution was dried at a temperature of 23°C to form a film.

The electrical characteristics of the EMFs were studied by impedance spectroscopy on an Agilent Technologies E5061B impedance analyzer in the frequency range of 1 Hz–100 MHz and on WK4042 in the frequency range of 0.1–1 MHz. A voltage of 0.25 V was applied to the measuring sensor.

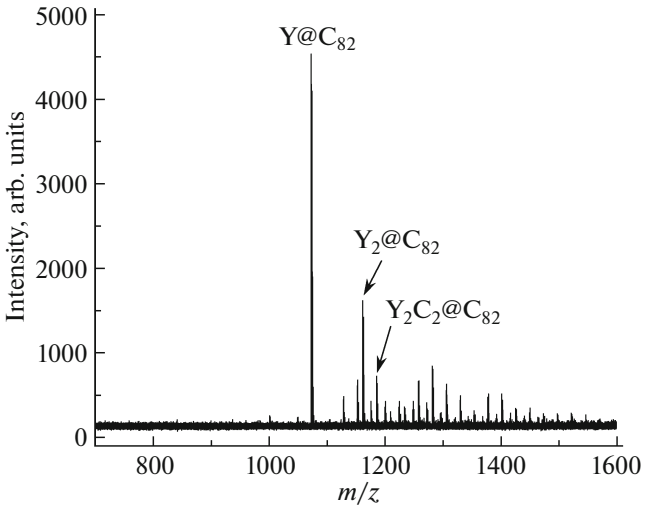


**Fig. 1.** Mass spectrum in positive ions of the chromatographic fraction.

The film elemental composition determined by X-ray photoelectron spectroscopy (XPS) was found to include 75.09 at % of carbon, 24.78 at % of oxygen, and 0.13 at % of yttrium. The XPS analysis of the C 1*s* line showed that the film consists of hydroxylated EMFs and higher fullerenes.

The frequency dependence of the absolute value of the impedance $|Z(f)|$ and phase $\varphi(f)$ was recorded at a temperature of 21°C. The data obtained allowed us to calculate the real $Z'(f) = |Z(f)|\cos\varphi(f)$ and imaginary $Z''(f) = |Z(f)|\sin\varphi(f)$ parts of the impedance and determine the effective capacitance $C_{eff}(f) = Z''(f)/(\omega Z'(f)R_{eff}(f))$ and effective resistance $R_{eff}(f) = Z'(f)(1 + Z''^2(f)/Z'^2(f))$ of the film [14]. Then, taking into account the calibration of the measuring sensor, frequency dependences of the real (ε') and imaginary (ε") parts of the permittivity [15] and real $Y' = Z'(f)/|Z(f)|$ and imaginary $Y'' = Z''(f)/|Z(f)|$ parts of the conductivity [14] were calculated (Figs. 2a, 2b, respectively).

It can be seen in Fig. 2 that the film exhibits the high values of both the real (ε') and imaginary (ε") parts of the permittivity in the low-frequency region, which is indicative of the occurrence of processes of motion and accumulation of electric charges, specifically, protons [16]. The sample has a noticeable real part of the conductivity *Y'*, which has a value of ~3 × $10^{-6}$ $\Omega^{-1}$ in the low-frequency region and, with an increase in frequency, attains ~$10^{-4}$ $\Omega^{-1}$. The growth of the imaginary part of the conductivity $Y''(f)$ at high frequencies is mainly determined by the effective capacitance $Y''(f) = 2\pi f C_{eff}(f)$.

The frequency-dependent sample resistance is most likely related to the hopping conductivity, which is confirmed by an increase in the real part of the conductivity *Y'* at high frequencies [17]; the real part of the conductivity weakly changes with frequency up to 1 MHz and then increases (Fig. 2b). This is typical of many heterogeneous materials with the hopping or polaron conductivity.

A minor variation in the *Y"* value with an increase in frequency to $10^3$ Hz is caused by the motion of carriers between electrodes in the bulk of the film. At low frequencies, carriers have enough time to move, following the field variation, so *Y"* takes its minimum value and ε', its maximum value. The minimum frequency starting with which *Y"* begins growing linearly with increasing frequency is usually considered to be the beginning of the low-frequency region where carriers can move between electrodes.

The electrical processes of polarization and charge transport in the sample under study can be observed in the resistance hodograph [9, 18] built in the form of the dependence of the imaginary impedance part *Z"* on the real impedance part *Z'* (Fig. 3). Each hodograph point corresponds to a certain frequency and the arrow shows the frequency increases direction.

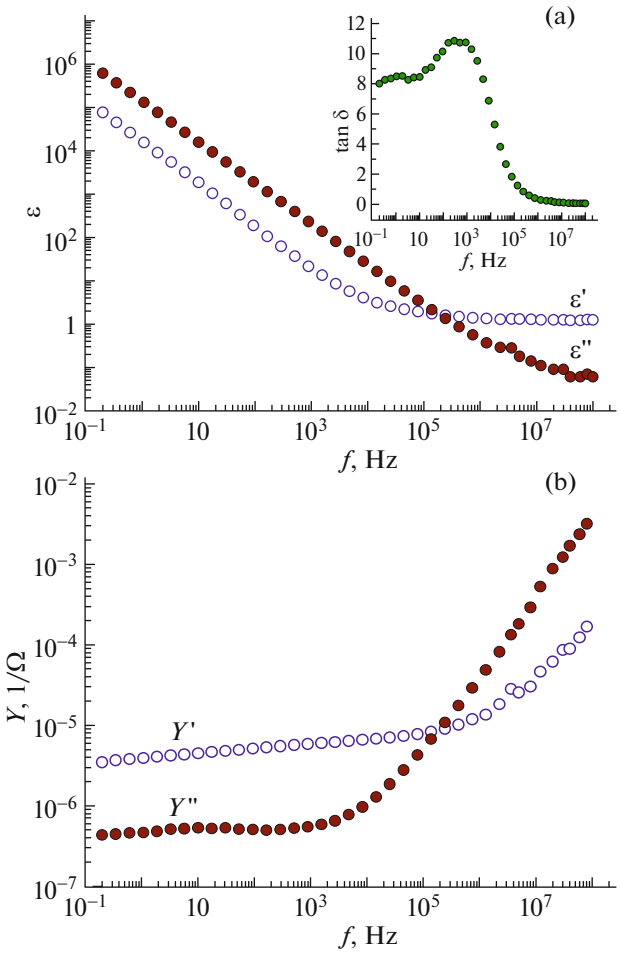


**Fig. 2.** Frequency dependence of (a) the real (ε') and imaginary (ε") parts of the permittivity and (b) the real (*Y'*) and imaginary (*Y"*) parts of the conductivity.

The hodograph consists of a circular arc and the so-called beam. The former corresponds to the intrinsic geometric capacitance of a measuring cell. The inflection point between these portions corresponds to the frequency at which *Y"* starts growing. In addition, this point corresponds to the maximum proton conductivity of the film [16]. Knowing the geometrical sizes of the film, we determined its proton conductivity, which was found to be ~5 × $10^{-3}$ $(\Omega\ cm)^{-1}$. The existence of carrier polarization on the electrodes can be proved by adding a dc bias to the measuring ac signal. This results in the full compensation of the potential barrier (plot *2* in Fig. 3).

The hysteresis on the *I–V* characteristic of the film arises because of accumulation of carries at the electrodes. The charge is retained for some time and induces an electric field directed opposite to the external field. With each next cycle, this reduces the slope

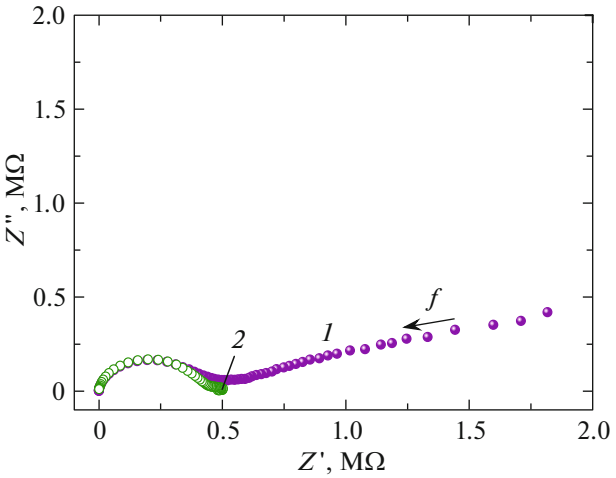


**Fig. 3.** Resistance hodograph of the film in the frequency range of 0.1 Hz–3 MHz (*1*) without dc bias and (*2*) under a dc bias of 2 V.

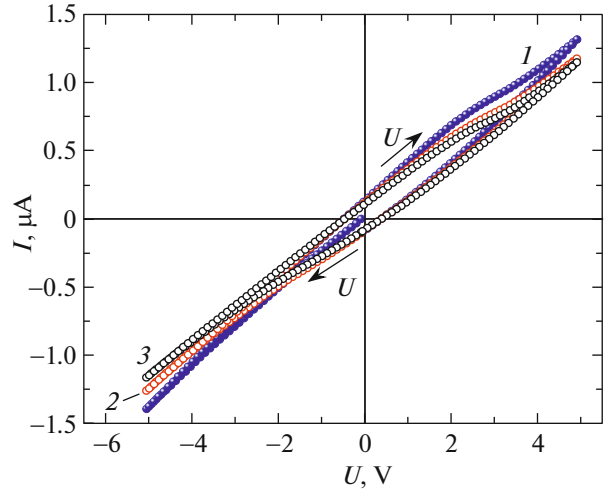


**Fig. 4.** *I–V* characteristic of the film. Each cycle begins with zero. Arrows show the voltage variation direction. (*1*) First cycle, (*2*) second cycle, and (*3*) third cycle.

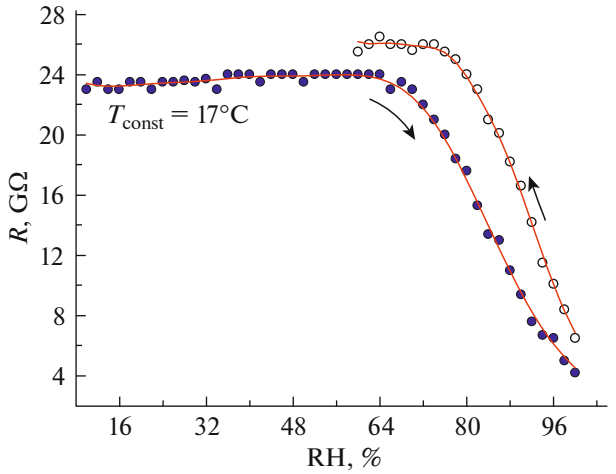


**Fig. 5.** Effect of the relative air humidity on the film resistance.

of the *I–V* curve relative to the abscissa axis; i.e., the film resistance increases.

The resistance of the film at a dc current as a function of the relative air humidity at a constant volume and temperature is shown in Fig. 5. Up to a humidity of 64%, the resistance is almost invariable. A further increase in the humidity leads to a sharp decrease in the resistance in accordance with the linear law. There is some hysteresis, which is possibly related to the slow penetration of water into the bulk of the film.

In view of the aforesaid, the investigated film sample should be considered as a spatially inhomogeneous structure, which can be strongly polarized in an ac electric field, which leads to the occurrence of anomalously large internal capacitances and conductivities.

The ferroelectric properties of the film were examined by the Positive Up Negative Down (PUND) method [19]. The investigations revealed a residual polarization of 0.136 μC. With regard to the film thickness, the value is $P_r \sim 0.75$ μC/cm$^2$.

A study of the impedance characteristics of the film based on hydroxylated EMFs with Y showed that the substance has the ε' value attaining $10^4$ and an ε'' value of $\sim 10^5$ at frequencies near 10 Hz. The conductivity of the investigated film is estimated as $5 \times 10^{-3}$ (Ω cm)$^{-1}$. The measurements showed that the EMF-based film with Y is a ferroelectric with a residual polarization of $P_r \approx 0.75$ μC/cm$^2$. Based on the results obtained, we may conclude that such important parameters of the products based on hydroxylated EMFs with Y as the ionic conductivity and ferroelectric properties depend on the amount of physically bound water in the material, i.e., on a technique used for fabricating the product and the operational environment.

## REFERENCES

1. R. B. Ross, C. M. Cardona, D. M. Guldi, S. G. Sankaranarayanan, M. O. Reese, N. Kopidakis, J. Peet, B. Walker, G. C. Bazan, E. van Keuren, B. C. Holloway, and M. Drees, Nat. Mater. **8**, 208 (2009).
2. W. Harneit, Phys. Rev. A **65**, 032322 (2002).
3. S. Keshri and B. L. Tembe, J. Chem. Phys. **146**, 074501 (2017).
4. H. C. Dorn and P. P. Fatouros, Nanosci. Nanotechnol. Lett. **2**, 65 (2010).
5. Z. Chen, R. Mao, and Y. Liu, Curr. Drug Metabolism **13**, 1035 (2012).
6. M. Rudolf, S. Wolfrum, D. M. Guldi, L. Feng, T. Tsuchiya, T. Akasaka, and L. Echegoyen, Chem. Eur. J. **18**, 5136 (2012).
7. M. E. Rincón, R. A. Guirado-López, J. G. Rodríguez-Zavala, and M. C. Arenas-Arrocena, Solar Energy Mater. Solar Cells **87**, 33 (2005).
8. A. L. Shakhmin, S. V. Murashov, N. V. Baranov, and M. A. Khodorkovskii, Phys. Solid State **40**, 150 (1998).
9. O. Gunnarsson, Rev. Mod. Phys. **69**, 575 (1997).

10. G. Churilov, A. Popov, N. Vnukova, A. Dudnik, N. Samoylova, and G. Glushenko, Fullerenes, Nanotubes, Carbon Nanostruct. **24**, 675 (2016).
11. G. N. Churilov, W. Kratschmer, I. V. Osipova, G. A. Glushenko, N. G. Vnukova, A. L. Kolonenko, and A. I. Dudnik, Carbon **62**, 389 (2013).
12. K. Akiyama, T. Hamano, Y. Nakanishi, E. Takeuchi, S. Noda, Z. Wang, S. Kubuki, and H. Shinohara, J. Am. Chem. Soc. **134**, 9762 (2012).
13. L. Y. Chiang, R. B. Upasani, J. W. Swirczewski, and S. Soled, J. Am. Chem. Soc. **115**, 5453 (1993).
14. *Impedance Spectroscopy Theory, Experiment, and Applications*, Ed. by E. Barsoukov and J. R. Macdonald (Wiley, Hoboken, NJ, 2005).
15. D. K. Pradhan, R. N. P. Choudhary, and B. K. Samantaray, Int. J. Electrochem. Sci. **3**, 597 (2008).
16. K. Hinokuma and M. Ata, J. Electrochem. Soc. **150**, 1.A112 (2003).
17. G. F. Neumark, Phys. Rev. B **20**, 1519 (1979).
18. H. Yang, C. Lu, Z. Liu, H. Jin, Y. Che, M. M. Olmstead, and A. L. Balch, J. Am. Chem. Soc. **130**, 17296 (2008).
19. *Ferroelectrics—Physical Effects*, Ed. by M. Lallart (InTech, Rijeka, 2011), p. 77.

*Translated by E. Bondareva*